

# Reactive In-Air Clothing Manipulation with Confidence-Aware Dense Correspondence and Visuotactile Affordance

Anonymous Author(s)

Affiliation

Address

email

1           **Abstract:** Manipulating clothing is challenging due to their complex, variable  
2 configurations and frequent self-occlusion. While prior systems often rely on  
3 flattening garments, humans routinely identify keypoints in highly crumpled and  
4 suspended states. We present a novel, task-agnostic, visuotactile framework that  
5 operates directly on crumpled clothing—including in-air configurations that have  
6 not been addressed before. Our approach combines global visual perception with  
7 local tactile feedback to enable robust, reactive manipulation. We train dense vi-  
8 sual descriptors on a custom simulated dataset using a distributional loss that cap-  
9 tures cloth symmetries and generates correspondence confidence estimates. These  
10 estimates guide a reactive state machine that dynamically selects between folding  
11 strategies based on perceptual uncertainty. In parallel, we train a visuotactile grasp  
12 affordance network using high-resolution tactile feedback to supervise grasp suc-  
13 cess. The same tactile classifier is used during execution for real-time grasp vali-  
14 dation. Together, these components enable a reactive, task-agnostic framework for  
15 in-air garment manipulation, including folding and hanging tasks. Moreover, our  
16 dense descriptors serve as a versatile intermediate representation for other plan-  
17 ning modalities, such as extracting grasp targets from human video demonstra-  
18 tions, paving the way for more generalizable and scalable garment manipulation.

19           **Keywords:** Deformable Object Manipulation, Dense Correspondence Learning,  
20 Confidence-Aware Planning, Visuotactile Perception

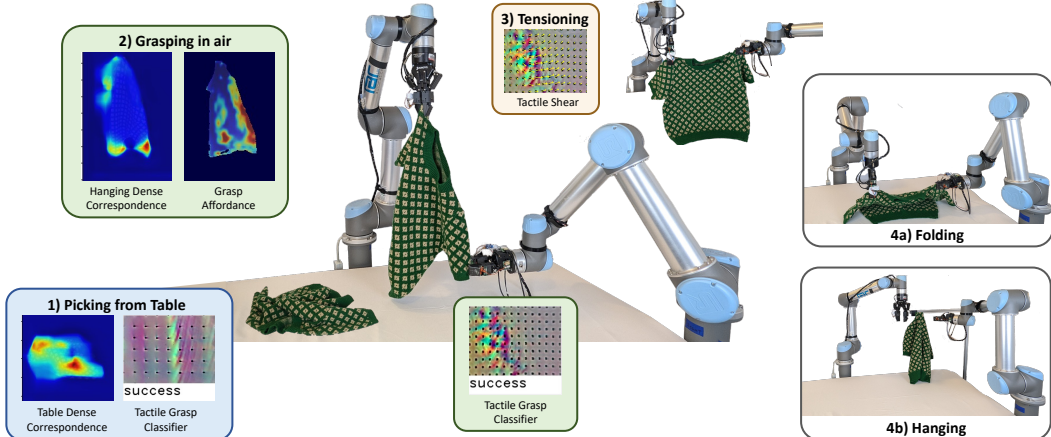


Figure 1: **Overview of visuotactile garment manipulation system.** Our framework integrates dense visual correspondence, visuotactile grasp affordance prediction, tactile grasp evaluation, and tactile tensioning for manipulating garments in crumpled configurations, both on a table-top and in-air. By leveraging a confidence-aware, reactive architecture and a task-agnostic representation, the system supports a variety of manipulation tasks—including folding and hanging.

21 **1 Introduction**

22 Deformable object manipulation remains a major challenge in robotics, since strategies developed  
23 for rigid objects often fail to transfer. Deformable objects occupy infinite-dimensional configuration  
24 spaces and exhibit high model uncertainty, making accurate state estimation and dynamics prediction  
25 difficult. Although simulation-based models exist, they are typically computationally intensive and  
26 insufficiently inaccurate for real-time control. In this work, we focus on garment manipulation,  
27 where real-world complexities—such as self-occlusion, intra-class variation, and diverse material  
28 dynamics—further complicate perception and control.

29 Existing approaches typically fall into two extremes: full-state estimation, which is expensive, or  
30 task-specific grasp predictors, which lack generalizability. To bridge this gap, we propose a pose-  
31 and instance-agnostic, confidence-aware representation using dense visual descriptors that estab-  
32 lishes pixel-wise correspondences between crumpled garments and canonical flat configurations.  
33 Trained on highly deformed states of detailed simulated shirts, our model can directly identify corre-  
34 spondences for shirts crumpled on a table and suspended in the air—a setting that, to our knowledge,  
35 has not been previously addressed.

36 Instead of the traditional contrastive loss, we use a distributional loss that models garment symme-  
37 tries and produces confidence estimates for each correspondence. These confidence scores inform  
38 whether a keypoint should be grasped or deferred, which is critical for operating under severe occlu-  
39 sion. We integrate this representation into a visuotactile manipulation system, using high-resolution  
40 tactile sensing to (1) supervise grasp affordance learning, (2) validate grasp success during execu-  
41 tion, and (3) enable closed-loop tensioning during folding. These components work together within  
42 a reactive framework that adapts folding and hanging strategies to garments of varying geometries,  
43 without requiring full-state estimation or flattening.

44 We make the following key technical contributions:

- 45 • **Parametrizable Simulator:** A custom simulator with realistic hem features and parameterized  
46 variations to enable correspondences across different shirt geometries.
- 47 • **Dense Representation:** Pixel-wise correspondences across challenging states using a distribu-  
48 tional loss to capture symmetries and provide confidence estimates.
- 49 • **Visuotactile Affordance:** Grasp affordance network trained in simulation and fine-tuned using  
50 tactile supervision.
- 51 • **Cloth Manipulation System:** A reactive visuotactile framework combining dense correspon-  
52 dences, affordances, and tactile sensing for confidence-aware in-air folding and hanging.

53 **2 Related Works**

54 Most previous cloth manipulation work focuses on task-specific pipelines, including flattening [1, 2],  
55 folding [3, 4, 5], dressing [6, 7], and recently hanging [8, 9, 10, 11]. These systems typically use  
56 incremental pick-and-place motions against a table [12, 13, 5, 14], and many focus on rectangular  
57 cloth, rather than garments.

58 Learning-based approaches can be quite successful at specific tasks. Labeling a real-world de-  
59 formable object dataset is challenging [15, 9], so most learning works are trained in simulation.  
60 However, the sim2real gap remains a challenge—we address this for our grasp affordance network  
61 by extending [16], fine-tuning using tactile classifiers to determine grasp success on the robot. Be-  
62 havior cloning approaches [8] have shown impressive results on tasks like tying shoelaces and hang-  
63 ing shirts, but require thousands of expert teleoperated demonstrations per task. In contrast, our  
64 system enables one- or few-shot generalization abilities and can reuse a shared object-centric repre-  
65 sentation across tasks.

66 **Perception and Representation** Early cloth manipulation work relies on corner detection or ridge  
67 detection [17] to determine grasp points [18]. However, finding other more specific local features

68 often requires first flattening the cloth [12, 19, 14, 1] or hanging it from specific grasp points [4, 20, 3]  
69 to avoid self-occlusion. Some works determine the global state of the cloth [21, 22, 23], but full-  
70 state inference is computationally expensive. In contrast, we use dense pixel-wise correspondences  
71 to directly localize task-relevant points in both crumpled table-top and in-air configurations.

72 **Dense Descriptors** Dense visual descriptors have been used to learn pixel-level correspondences  
73 across object views [24, 25]. Florence et al. [26] introduce dense object descriptors for task-agnostic  
74 manipulation, with follow-up work applying them to deformable objects [5, 27, 28]. Prior cloth-  
75 specific applications use contrastive loss [5, 28], but Ganapathi et al. [29] use multimodal distri-  
76 butional loss [30] to model symmetry and uncertainty on ropes and square cloths. We extend this  
77 to garments, training on highly crumpled configurations and enabling in-air correspondence predic-  
78 tion—a capability not previously addressed. Our approach further differs from garment manipula-  
79 tion in [28] because of our use of reactive control, made possible by confidence-aware descriptors  
80 and tactile feedback. We also demonstrate that our dense descriptors can act as an intermediate rep-  
81 resentation for different planning modalities. For example, Huang et al. [31] uses DinoV2 [32] and  
82 a vision-language model to determine constraints; our descriptors could find keypoint candidates to  
83 better support manipulation in more crumpled states.

### 84 3 Methods

#### 85 3.1 Dataset Generation in Simulation

86 We use Blender 4.2 [33] to simulate a wide variety of shirt geometries and deformations, gener-  
87 ating a large RGB-D dataset (1500 scenes) for training. In addition to parameterizing the overall  
88 geometries, we use [34] to incorporate hems, stitches, and sewing seams into our shirts to mimic  
89 realistic garments, enhancing visual realism and providing key features helpful for correspondence.  
90 Our method incorporates these finer details while preserving consistent vertex indexing across shirts,  
91 enabling descriptors to align with a canonical template regardless of geometry, without relying on  
92 sparse skeleton keypoints as in [28]. Figure 2 shows some of the parameters and shirt configurations  
93 we randomize to generate our dataset.

94 Scene generation mimics real-world camera setups, with three cameras arranged radially around the  
95 hanging shirt, with added pose noise and varied lighting conditions to enhance dataset diversity. For  
96 each hanging scene, a shirt is hung from a random mesh point and the world coordinates and pixel  
97 locations of the deformed mesh vertices are saved. For each table scene, a randomly positioned flat  
98 shirt is repeatedly grasped from random points and repositioned multiple times. This setup captures  
99 rich, diverse data across garment shapes, crumpled configurations (hanging and table), and visual  
100 contexts, enabling robust correspondence learning between different poses and shirt instances. See  
101 Appendix for further simulation details.

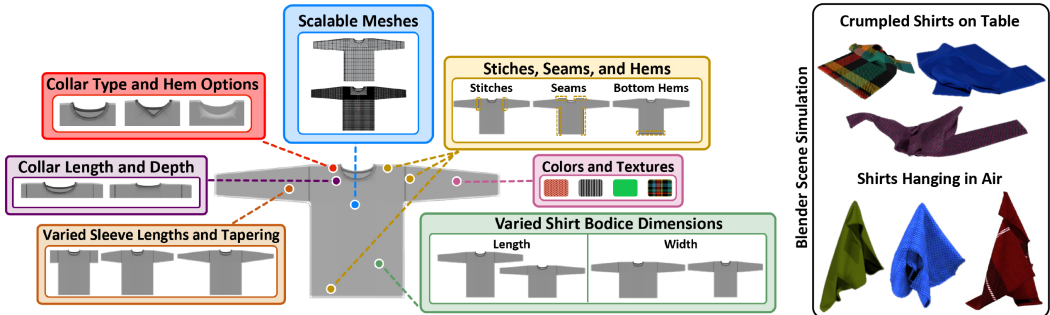


Figure 2: **Generating a simulated shirt dataset.** Blender 4.2 is used to simulate deformed shirts. Our animation pipeline allows flexibility in shirt geometries with the addition of realistic, key features like seams and hems often found on real shirts. A consistent vertex indexing across the shirt dataset is used, allowing alignment with a canonical template.

102 **3.2 Dense Correspondence with Distributive Loss**

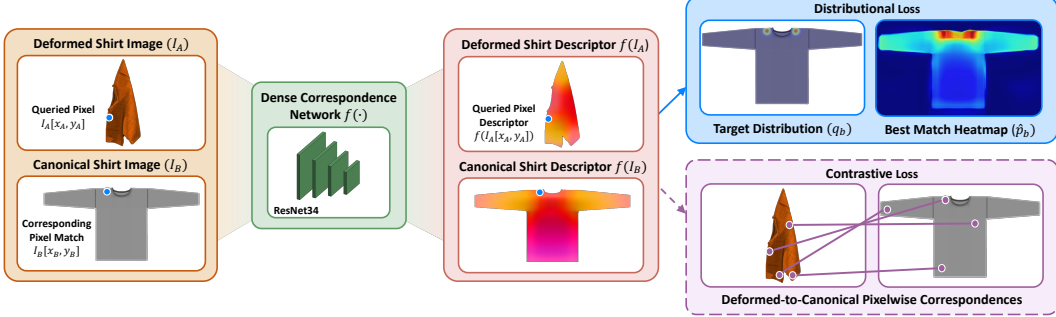


Figure 3: **Training dense correspondence in simulation.** Given two images  $I_a$  and  $I_b$ , and a matching relation  $((x_a, y_a) \longleftrightarrow \{(x_b, y_b), (x'_b, y'_b)\})$ , we train a CNN model  $f$  to compute dense object descriptors. When supervising with distributional loss, we define a multimodal Gaussian target distribution  $q_b$  with symmetrical modes over pixels corresponding to the queried point. We compute the probability distribution estimation  $\hat{p}_{b_i}$  over image  $I_b$  using  $f(I_a)[x_a, y_a]$  and  $f(I_b)$ . Training minimizes the KL divergence between  $q_b$  and  $\hat{p}_{b_i}$ . In the contrastive loss case, the model learns to push discrete pixel matches closer together in pixel space and non-matches further apart.

103 We aim to learn dense pixel-wise correspondences between images of deformable objects in crumpled  
104 and flattened configurations. Given an RGB image  $I \in \mathbb{R}^{W \times H \times 3}$ , we define a mapping  
105  $f : \mathbb{R}^{W \times H \times 3} \rightarrow \mathbb{R}^{W \times H \times d}$  that assigns a  $d$ -dimensional descriptor to each pixel in  $I$ . This de-  
106 scriptor space allows correspondences to be established by comparing descriptors across images.

107 **Contrastive Loss** Contrastive methods, as used by [26, 5, 28], supervise this mapping by sampling  
108 pairs of matching and non-matching pixels across images. For a query pixel  $u_a = (x_a, y_a)$  in image  
109  $I_a$  and a candidate pixel  $u_b = (x_b, y_b)$  in image  $I_b$ , the descriptor distance  $D(I_a, u_a, I_b, u_b) =$   
110  $\|f(I_a)(u_a) - f(I_b)(u_b)\|_2$  is minimized for matching pairs and pushed apart for non-matching pairs.  
111 This enforces one-to-one correspondences but struggles with ambiguities caused by symmetries  
112 or occlusions, which are common in deformable objects. Symmetric Pixel-wise Contrastive Loss  
113 (SPCL) [29] extends this approach to support symmetric correspondences, allowing multiple valid  
114 matches per query pixel. However, they found the results to be unstable, and the discrete matches  
115 resulted in discontinuity issues. We will compare our network to these contrastive baselines.

116 **Distributional Loss** To address these limitations, we adopt the distributional formulation from [29],  
117 which directly models uncertainty over correspondences. Instead of supervising individual descrip-  
118 tor pairs, the network predicts a full probability distribution over possible matches. Specifically, we  
119 define an estimator  $\hat{p}_b(x_i, y_j | I_a, I_b, x_a, y_a)$  that outputs the probability that each pixel  $(x_i, y_j) \in I_b$   
120 corresponds to a given query pixel  $(x_a, y_a) \in I_a$ . This estimator is defined as:

$$\hat{p}_b(x_i, y_j | I_a, I_b, x_a, y_a) = \frac{\exp \|f(I_a)[x_a, y_a] - f(I_b)[x_i, y_j]\|_2^2}{\sum_{i', j'} \exp \|f(I_a)[x_a, y_a] - f(I_b)[x_{i'}, y_{j'}]\|_2^2} \quad \forall (x_i, y_j) \in I_b \quad (1)$$

121 The target distribution  $q_b$  is a multimodal isotropic Gaussian defined over  $I_b$ , with standard deviation  
122  $\sigma$  and modes centered at the ground-truth correspondence pixels, allowing the network to represent  
123 multiple valid matches and capture ambiguities from symmetry.

124 The descriptor mapping  $f$  is implemented using ResNet34. The network is optimized by minimizing  
125 the Kullback-Leibler (KL) divergence between the predicted distribution  $\hat{p}_{b_i}$  and the target distribu-  
126 tion  $q_{b_i}$  for each query pixel. Here,  $\hat{p}_{b_i}$  is the predicted correspondence distribution over  $I_b$  for the  
127  $i$ -th query pixel (computed using Equation 1), and  $q_{b_i}$  is the corresponding target distribution. Fig-  
128 ure 3 shows a training example. At each iteration, we choose an image of a randomized crumpled  
129 shirt and compare it to the canonical one. We query 50 randomly sampled points on the crumpled  
130 shirt per iteration.

131 Note that  $I_b$  is always the canonical shirt image, meaning that we compute both the target and  
132 estimated distributions over the canonical shirt. A smooth Gaussian target distribution works over  
133 the canonical shirt because it does not have occlusions and distortions of the crumpled shirt. Defining  
134 the target distribution over the crumpled shirt would be useful for training the network in both  
135 directions, but is unfeasible in this framework.

### 136 3.3 Visuotactile Grasp Affordance

137 Training a general garment grasp affordance network is more challenging than for simpler de-  
138 formable objects like towels. In [16], the network was fine-tuned on a single towel with consis-  
139 tent material properties and dynamics. However, in this case, affordance must generalize across  
140 a wide range of geometries and material rigidities. As in [16], we only use side grasps to reduce  
141 computational complexity. While grasp classifiers are trained for both grippers (as required by the  
142 larger system), affordance training is performed only for right-arm grasps, with left-arm affordance  
143 approximated by horizontally flipping inputs and outputs.

144 **Tactile Classifier** To assess grasp quality, we train tactile classifiers to distinguish between suc-  
145 cessful grasps, grasps with too little fabric (which are prone to slip), and grasps with excess layers  
146 (indicating more fabric than intended). We concatenate five evenly-spaced tactile depth images from  
147 the grasp attempt as input to our network. Our tactile datasets includes 350 grasps across approxi-  
148 mately 20 shirts, with limited augmentations (two per input).

149 **Training Affordance in Simulation** We use the same U-Net [35] architecture as [16] for affordance  
150 prediction. The input to the network is a depth image of the hanging garment, and the output is an  
151 affordance heatmap over the image. Ground-truth affordance labels are computed per pixel via  
152 geometric analysis, leveraging full access to the cloth state in simulation. Specifically, each pixel  
153 is labeled based on gripper reachability, collision avoidance, and the number of fabric layers inside  
154 the gripper (restricted to two or fewer). These criteria are all explicitly checked in simulation, but  
155 the tactile classifier implicitly verifies these qualities on the robot. The simulated dataset consists of  
156 300 unique cloth configurations, each rotated in increments of 30°, yielding a total of 3,600 images.

157 **Fine-tuning on the Robot** We collect 8,500 grasp points for real-world fine-tuning to capture the  
158 greater variety of shirt dynamics and configurations compared to the simulated environment. Fine-  
159 tuning can easily overfit the real grasp dataset because the loss only applies to one pixel at a time.  
160 Furthermore, the tactile classifier cannot reliably determine whether the grasped region corresponds  
161 to the intended visual target. As a result, non-reachable pixels can yield positive tactile signals due  
162 to inadvertently grasping cloth in front of the target. To help address these challenges, our loss  
163 includes neighboring pixels to broaden supervision, along with regularization terms such as spatial  
164 smoothness penalties, simulation consistency constraints, and weight decay.

### 165 3.4 System Setup

166 Our bimanual system consists of two UR5 robots, both equipped with parallel-jaw grippers mounted  
167 with GelSight Wedge tactile sensors [36]. A Kinect Azure camera is used to capture RGB-D images.

### 168 3.5 In-Air Garment Manipulation

169 **Folding with Confidence-based State Machine** Unlike prior garment folding approaches that rely  
170 on fixed canonical keypoints [5, 28] for folding on a table, our system enables reactive in-air folding  
171 by dynamically selecting grasp points based on real-time confidence estimates and recovering from  
172 failures using tactile reactivity. The system starts by picking the shirt up from the table (looking for  
173 high-confidence correspondence regions), and all subsequent grasps are performed in air.

174 At each grasp attempt, the robot can query from three canonical regions (shoulder, sleeve, bottom)  
175 using our distributional dense correspondence network to generate confidence-weighted heatmaps.  
176 A grasp is executed only if both the correspondence confidence and grasp affordance (for hang-  
177 ing grasps) exceed predefined thresholds. Otherwise, the robot rotates the garment by 30° and re-

178 evaluates, ensuring robust grasp point selection across four folding strategies (shoulder-to-shoulder,  
 179 bottom-to-bottom, sleeve-to-sleeve, sleeve-to-bottom) (See Appendix for details).

180 Grasp success is validated by tactile sensing (confirming fabric contact). If a grasp fails, the robot  
 181 rotates and retries without releasing the garment. We use vision to ensure that the cloth is still in  
 182 grip after moving the grippers. If no pixel meets the threshold requirements, the robot grasps the  
 183 lowest available high affordance point to change configurations and encourage the cloth to unfurl.  
 184 Once two confident grasp points are secured, the robot tensions the shirt (detecting shear via marker  
 185 tracking on tactile sensors) and performs the rest of the fold motions open-loop.

186 **Hanging** We demonstrate hanging by picking collar or shoulder from the table and in the air. After  
 187 securing both grasps, the robot moves open-loop to a peg. Hanging success is evaluated by grasp  
 188 regions and whether the cloth stays on the peg.

## 189 4 Results

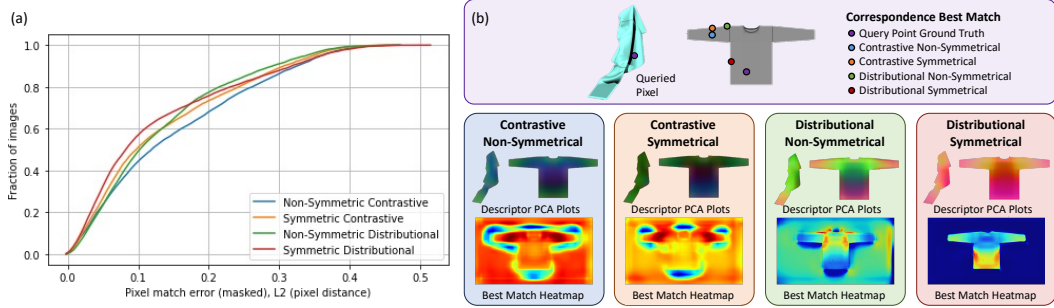


Figure 4: **(a) Cumulative pixel match error curves comparing contrastive and distributional training, with and without symmetric supervision along with (b) illustrative example.** The networks were trained on a combined dataset of hanging and table shirts and (a) shows performance on an unseen hanging test set. Higher curves indicate better performance. For each network, we show the predicted best pixel match for a queried point on a crumpled simulated shirt (b). We also provide PCA visualizations of the dense descriptors in both the canonical and crumpled states, alongside the corresponding match heatmaps. Note that contrastive heatmaps are normalized between 0 and 1 for visualization, while distributional heatmaps represent true correspondence probabilities.

190 **Dense Correspondence** Most dense descriptor methods use contrastive one-to-one training [26, 5,  
 191 28], which fails to capture symmetries or spatial relationships beyond binary matches. Quantitative  
 192 results (Fig. 5) show similar cumulative pixel errors between contrastive and distributional models,  
 193 but distributional models consistently outperform contrastive ones across nearly all error thresholds.  
 194 Qualitatively, contrastive loss struggles ambiguous structures, often collapsing descriptors along the  
 195 entire sleeve or confusing sleeves with the shirt bottom (as seen in PCA visualizations). In contrast,  
 196 distributional loss supervises the model to predict a full probability distribution, enforcing spatial  
 197 consistency. Explicit symmetry supervision further improves performance (Fig. 5), especially at  
 198 low error thresholds, by encouraging multimodal correspondences in symmetric regions.

199 We found that including occlusions during training did not significantly affect performance in simu-  
 200 lation, but helped improve performance on real data, likely due to masking artifacts. More detailed  
 201 analysis of network parameters can be found in the Appendix.

202 On real robot hanging images, we evaluate our network by defining classification zones on the  
 203 canonical shirt (see Appendix). When querying points from a crumpled hanging shirt (forward  
 204 direction), the best hanging-only network classified the correct region 73.3% of the time, while the  
 205 best combined network (trained on both table and hanging data) achieved 62.2% accuracy, while  
 206 exhibiting lower overall confidence. Applying a confidence threshold, the combined network made  
 207 correct, confidence-aware decisions (avoiding incorrect labels) 68.9% of the time. In the inverse  
 208 direction (querying from the canonical shirt), the combined network correctly identified the region  
 209 41.7% of the time and made safe, confidence-aware decisions 70.8% of the time. Some canonical

210 points were occluded in the crumpled image, making low confidence the correct outcome for these  
211 cases. On table scenes, the correct correspondence region was identified 70% of the time, and a safe  
212 decision—either correct or low-confidence—was made 80% of the time in 20 trials.

213 **Visuotactile Grasp Affordance** Our tactile grasp classifier achieves 99.7% accuracy on the right  
214 arm (used for tactile supervision) and 98.8% on the left. Thin, flat shirts are the most challenging to  
215 classify. To evaluate affordance prediction, we collect 125 human-labeled grasp points where each  
216 point appeared potentially graspable to a human observer. We compare our fine-tuned affordance  
217 network against two baselines: (1) Sim2Real, trained in simulation and directly deployed, and (2)  
218 Real2Real, trained solely on robot data. Networks are evaluated offline using precision@k [37],  
219 a metric suitable for our unbalanced test set that avoids the need for a fixed threshold. We report  
220 precision@80, corresponding to the 80 successful grasps among the 125 test points. The results  
221 are 71.3% for Sim2Real, 75.0% for Real2Real, and 76.3% for our fine-tuned network. Sim2Real  
222 performs worst due to discrepancies between simulated and real-world dynamics. While the fine-  
223 tuned and Real2Real networks achieve similar precision, qualitative analysis shows that Real2Real  
224 tends to be overconfident in incorrect predictions, particularly in less ambiguous cases not well-  
225 represented in the test set (see Appendix).

226 **Combined System** We evaluate grasping performance across four garment regions—sleeve, bot-  
227 tom, shoulder, and collar—using two networks: one trained solely on hanging data and another on  
228 a combined table and hanging dataset. For each category, we perform 10 grasp attempts per net-  
229 work, recording outcomes as success, failure, or below confidence threshold. Failures are further  
230 categorized as correspondence errors or affordance errors. In this experiment, we place the shirt  
231 in configurations where we expect graspable regions to emerge after rotation. Table 1 summarizes  
232 rates for overall success, correspondence success (excluding bad affordance grasps), low-confidence  
233 rates, and total failure rates for each network and region.

234 The collar region consistently achieves higher confidence and success rates, likely due to its distinc-  
235 tive geometry. In contrast, the bottom region has the lowest confidence rates, reflecting its visual  
236 ambiguity and the increased difficulty of finding good affordance grasps from folding in on itself.  
237 The hanging network performs marginally better overall, but the combined network adds critical  
238 flexibility by supporting table grasps. Importantly, during folding, we query three candidate grasp  
239 points for the initial grasp, requiring confidence in only one to proceed. Subsequent grasps occur in  
240 easier, more unfurled configurations.

Category	Successful Grasp (%)		Corr. Success (%)		Low Conf. (%)		Failed Grasp (%)	
	Hang	Comb	Hang	Comb	Hang	Comb	Hang	Comb
Sleeve	60	40	80	60	10	10	30	50
Bottom	40	10	90	90	40	80	20	10
Shoulder	40	60	100	100	60	20	0	20
Collar	80	80	90	90	0	0	20	20

Table 1: **Grasping results using dense correspondence and grasp affordance across shirt categories for hanging and combined (hanging + table) dataset networks.** Low-confidence out-  
comes, where the shirt completes a full rotation without finding a grasp point, are not counted as  
successful or failed grasps. They are still included when calculating correspondence success, since  
both networks are trained to be confidence-aware. Failed grasps are categorized as either correspon-  
dence or affordance failures. Correspondence success rates exclude grasps that failed due to bad  
affordance predictions.

241 We found that our confidence-aware state machine was able to grasp viable folding points in 6 out of  
242 10 trials. Irrecoverable failure modes included correspondence failures, grabbing too much fabric,  
243 and grabbing diagonally across the shirt for sleeve-end grasps (despite masking out lowest points,  
244 see Appendix). Cloth slipping out was an occasional issue, but the system is able to recover. Our  
245 hanging system was successful in 7 out of 10 trials with all failures due to correspondence.

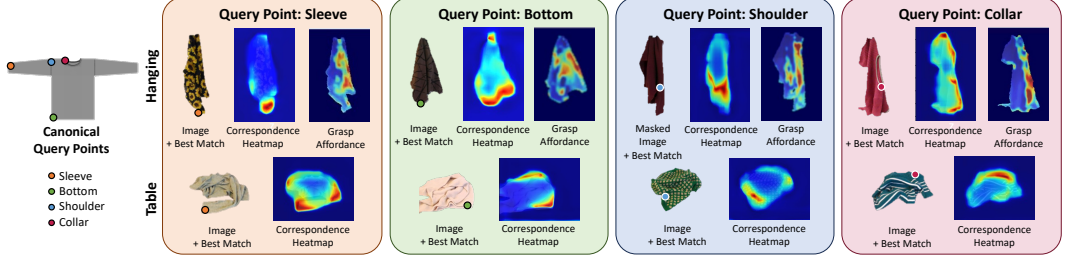


**Figure 5: Correspondence and affordance heatmaps for real images.** We show examples for both hanging and table configurations, with correspondence probability maps for four query types: sleeve, shoulder, collar, and bottom. For hanging images, we also show the grasp affordance heatmap. In the robot system, grasp points are selected where both correspondence and affordance exceed predefined confidence thresholds. Note that while training queries points on the crumpled shirt, the robot queries points on the canonical image.

## 246 5 Conclusion

247 We present a reactive visuotactile system for garment manipulation that integrates dense visual cor-  
 248 respondence, visuotactile grasp affordance, confidence-aware planning, and tactile feedback. Unlike  
 249 prior work constrained to table-top picking or reliant on flattening, our system supports in-air gar-  
 250 ment manipulation directly from crumpled states, guided by dense correspondences—a capability  
 251 not previously demonstrated in the field. This enables more flexible, human-like manipulation.

252 A core insight of our work is the importance of confidence-driven reactivity: by deferring low-  
 253 confidence actions and using tactile sensing for validation and correction, the system maintains  
 254 robustness under severe occlusion and uncertainty. This closed-loop approach bridges the gap be-  
 255 tween global visual context and local contact feedback, enabling reliable control even when full  
 256 object geometry is not observable.

257 Beyond task execution, our dense, confidence-aware representation serves as a generalizable inter-  
 258 mediate layer for higher-level planning frameworks. It provides a foundation for extracting grasp  
 259 targets from human video demonstrations (Fig 6, See Appendix for details), and has the potential to  
 260 interface with vision-language models [31] or symbolic planners. These directions open the door to  
 261 scalable, semantically-informed manipulation systems capable of adapting across garments, tasks,  
 262 and contexts.

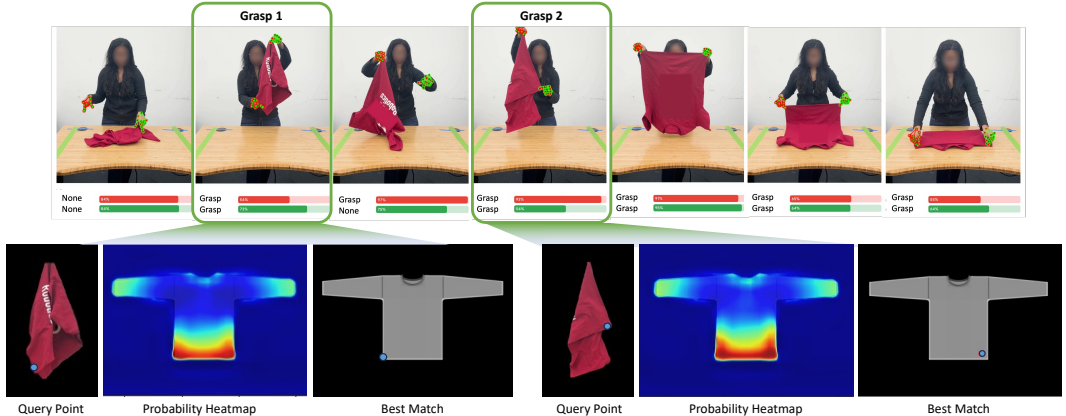


**Figure 6: Extracting grasp points from human video demonstrations.** We track hand gestures throughout the video to identify key moments. For each key frame, we use the tracked hand position to define a query point and retrieve the corresponding location on the canonical shirt using our dense correspondence model. This approach enables folding demonstrations to be interpreted as robot-executable instructions via our dense visual representation.

263 **6 Limitations**

264 While our system demonstrates strong potential for in-air garment manipulation, several areas  
265 present opportunities for further development. First, the generalizability of the dense correspon-  
266 dence network is limited by the features available in simulation. Although we incorporated realistic  
267 details such as seams, hems, and varied necklines, other common garment features—like hoods,  
268 buttons, zippers, and mixed patterns—are not yet modeled. Some of these could be added in future  
269 dataset expansions, while others may require advances in simulation tools. On out-of-distribution  
270 shirts (see Appendix), the network still captures general structure, but with lower confidence.

271 Second, we are able to achieve this performance with a single camera and exclusively side approach  
272 grasps, but expanding to additional viewpoints and enabling more grasp approach angles could im-  
273 prove coverage to access more high correspondence regions. Incorporating temporal information  
274 could further enable the system to track keypoints as they become accessible, supporting more flex-  
275 ible planning.

276 Finally, although the system is confidence-aware, the network occasionally overestimates its cer-  
277 tainty in challenging configurations. We experimented with auxiliary confidence prediction and  
278 KL-divergence metrics, but these did not significantly improve failure detection. Improving uncer-  
279 tainty estimation remains an important direction for future work.

280 **References**

- 281 [1] H. Ha and S. Song. Flingbot: The unreasonable effectiveness of dynamic manipulation for  
282 cloth unfolding. In *Conference on Robot Learning*, pages 24–33. PMLR, 2022.
- 283 [2] A. Canberk, C. Chi, H. Ha, B. Burchfiel, E. Cousineau, S. Feng, and S. Song. Cloth fun-  
284 nels: Canonicalized-alignment for multi-purpose garment manipulation, 2022. URL <https://arxiv.org/abs/2210.09347>.
- 285 [3] J. Maitin-Shepard, M. Cusumano-Towner, J. Lei, and P. Abbeel. Cloth grasp point detection  
286 based on multiple-view geometric cues with application to robotic towel folding. In *2010 IEEE*  
287 *International Conference on Robotics and Automation*, pages 2308–2315. IEEE, 2010.
- 288 [4] A. Doumanoglou, A. Kargakos, T.-K. Kim, and S. Malassiotis. Autonomous active recognition  
289 and unfolding of clothes using random decision forests and probabilistic planning. In *2014*  
290 *IEEE international conference on robotics and automation (ICRA)*, pages 987–993. IEEE,  
291 2014.
- 292 [5] A. Ganapathi, P. Sundaresan, B. Thananjeyan, A. Balakrishna, D. Seita, J. Grannen, M. Hwang,  
293 R. Hoque, J. E. Gonzalez, N. Jamali, K. Yamane, S. Iba, and K. Goldberg. Learning to smooth  
294 and fold real fabric using dense object descriptors trained on synthetic color images. *arXiv*,  
295 2020.
- 296 [6] F. Zhang and Y. Demiris. Learning garment manipulation policies toward robot-assisted dress-  
297 ing. *Science robotics*, 7(65):eabm6010, 2022.
- 298 [7] Z. Sun, Y. Wang, D. Held, and Z. Erickson. Force-constrained visual policy: Safe robot-  
299 assisted dressing via multi-modal sensing. *IEEE Robotics and Automation Letters*, 2024.
- 300 [8] T. Z. Zhao, J. Tompson, D. Driess, P. Florence, K. Ghasemipour, C. Finn, and A. Wahid. Aloha  
301 unleashed: A simple recipe for robot dexterity. *arXiv preprint arXiv:2410.13126*, 2024.
- 302 [9] W. Chen, D. Lee, D. Chappell, and N. Rojas. Learning to grasp clothing structural regions for  
303 garment manipulation tasks. In *2023 IEEE/RSJ International Conference on Intelligent Robots*  
304 and Systems (IROS), pages 4889–4895. IEEE, 2023.
- 305 [10] Y. Chen, S. Wei, B. Xiao, J. Lyu, J. Chen, F. Zhu, and H. Wang. Robohanger: Learning  
306 generalizable robotic hanger insertion for diverse garments. *arXiv preprint arXiv:2412.01083*,  
307 2024.
- 308 [11] W. Chen, K. Li, D. Lee, X. Chen, R. Zong, and P. Kormushev. Graphgarment: Learning  
309 garment dynamics for bimanual cloth manipulation tasks. *arXiv preprint arXiv:2503.05817*,  
310 2025.
- 311 [12] Y. Wu, W. Yan, T. Kurutach, L. Pinto, and P. Abbeel. Learning to manipulate deformable  
312 objects without demonstrations, 2019.
- 313 [13] R. Hoque, D. Seita, A. Balakrishna, A. Ganapathi, A. K. Tanwani, N. Jamali, K. Yamane,  
314 S. Iba, and K. Goldberg. VisuoSpatial foresight for multi-step, multi-task fabric manipulation,  
315 2020.
- 316 [14] X. Lin, Y. Wang, Z. Huang, and D. Held. Learning visible connectivity dynamics for cloth  
317 smoothing. In *Conference on Robot Learning*, pages 256–266. PMLR, 2022.
- 318 [15] J. Qian, T. Weng, L. Zhang, B. Okorn, and D. Held. Cloth region segmentation for robust grasp  
319 selection. In *IEEE International Conference on Intelligent Robots and Systems*, 2020. ISBN  
320 9781728162126. doi:10.1109/IROS45743.2020.9341121.
- 321 [16] N. Sunil, S. Wang, Y. She, E. Adelson, and A. R. Garcia. Visuotactile affordances for cloth  
322 manipulation with local control. In *6th Annual Conference on Robot Learning*, 2022. URL  
323 <https://openreview.net/forum?id=s6NEzqZKaP->.

- 325 [17] K. Yamazaki, K. Nagahama, and M. Inaba. Daily clothes observation from visible surfaces  
 326 based on wrinkle and cloth-overlap detection. In *MVA*, pages 275–278, 2011.
- 327 [18] B. Willimon, S. Birchfield, and I. Walker. Model for unfolding laundry using interactive per-  
 328 ception. In *IEEE International Conference on Intelligent Robots and Systems*, 2011. ISBN  
 329 9781612844541. [doi:10.1109/IROS.2011.6048796](https://doi.org/10.1109/IROS.2011.6048796).
- 330 [19] R. Hoque, K. Shivakumar, S. Aeron, G. Deza, A. Ganapathi, A. Wong, J. Lee, A. Zeng, V. Van-  
 331 houcke, and K. Goldberg. Learning to fold real garments with one arm: A case study in  
 332 cloud-based robotics research. *arXiv preprint arXiv:2204.10297*, 2022.
- 333 [20] M. Cusumano-Towner, A. Singh, S. Miller, J. F. O’Brien, and P. Abbeel. Bringing clothing  
 334 into desired configurations with limited perception. In *2011 IEEE international conference on*  
 335 *robotics and automation*, pages 3893–3900. IEEE, 2011.
- 336 [21] T. Tang, Y. Fan, H.-C. Lin, and M. Tomizuka. State estimation for deformable objects by point  
 337 registration and dynamic simulation. In *Intelligent Robots and Systems (IROS), 2017 IEEE*  
 338 *International Conference on*. IEEE, 2017.
- 339 [22] C. Chi and D. Berenson. Occlusion-robust deformable object tracking without physics simula-  
 340 tion. In *Intelligent Robots and Systems (IROS), 2019 IEEE International Conference on*. IEEE,  
 341 2019.
- 342 [23] C. Chi and S. Song. Garmentnets: Category-level pose estimation for garments via canonical  
 343 space shape completion. *CoRR*, abs/2104.05177, 2021. URL <https://arxiv.org/abs/2104.05177>.
- 345 [24] C. B. Choy, J. Gwak, S. Savarese, and M. Chandraker. Universal correspondence network.  
 346 *CoRR*, abs/1606.03558, 2016. URL <http://arxiv.org/abs/1606.03558>.
- 347 [25] T. Schmidt, R. A. Newcombe, and D. Fox. Self-supervised visual descriptor learning for dense  
 348 correspondence. *IEEE Robotics and Automation Letters*, 2017.
- 349 [26] P. R. Florence, L. Manuelli, and R. Tedrake. Dense object nets: Learning dense visual object  
 350 descriptors by and for robotic manipulation. *CoRR*, abs/1806.08756, 2018. URL <http://arxiv.org/abs/1806.08756>.
- 352 [27] P. Sundaresan, J. Grannen, B. Thananjeyan, A. Balakrishna, M. Laskey, K. Stone, J. E.  
 353 Gonzalez, and K. Goldberg. Learning rope manipulation policies using dense object de-  
 354 scriptors trained on synthetic depth data. *CoRR*, abs/2003.01835, 2020. URL <https://arxiv.org/abs/2003.01835>.
- 356 [28] R. Wu, H. Lu, Y. Wang, Y. Wang, and H. Dong. Unigarmentmanip: A unified framework for  
 357 category-level garment manipulation via dense visual correspondence. In *Proceedings of the*  
 358 *IEEE/CVF Conference on Computer Vision and Pattern Recognition (CVPR)*, June 2024.
- 359 [29] A. Ganapathi, P. Sundaresan, B. Thananjeyan, A. Balakrishna, D. Seita, R. Hoque, J. E. Gonza-  
 360 lez, and K. Goldberg. MMGSD: Multi-Modal Gaussian Shape Descriptors for Correspondence  
 361 Matching in 1D and 2D Deformable Objects. In *Intelligent Robots and Systems (IROS), 2020*  
 362 *IEEE International Conference on*, 2020.
- 363 [30] P. Florence. *Dense visual learning for robot manipulation*. PhD thesis, Massachusetts Institute  
 364 of Technology, 01 2020.
- 365 [31] W. Huang, C. Wang, Y. Li, R. Zhang, and L. Fei-Fei. Rekep: Spatio-temporal reasoning of  
 366 relational keypoint constraints for robotic manipulation. *arXiv preprint arXiv:2409.01652*,  
 367 2024.

- 368 [32] M. Oquab, T. Darcet, T. Moutakanni, H. Vo, M. Szafraniec, V. Khalidov, P. Fernandez, D. Haz-  
369 iza, F. Massa, A. El-Nouby, et al. Dinov2: Learning robust visual features without supervision.  
370 *arXiv preprint arXiv:2304.07193*, 2023.
- 371 [33] Blender Online Community. Blender. <https://www.blender.org/>, 2025. Version 4.2.
- 372 [34] A. Albisser. Procedural cloth sewing toolbox for blender 4.2+. <https://alexandrealbisser.gumroad.com/l/ProceduralSewingToolbox>, 2024. Software tool.
- 374 [35] O. Ronneberger, P. Fischer, and T. Brox. U-net: Convolutional networks for biomedical  
375 image segmentation. In *International Conference on Medical image computing and computer-  
376 assisted intervention*, pages 234–241. Springer, 2015.
- 377 [36] S. Wang, Y. She, B. Romero, and E. Adelson. Gelsight wedge: Measuring high-resolution  
378 3d contact geometry with a compact robot finger. In *2021 IEEE International Conference on  
379 Robotics and Automation (ICRA)*, pages 6468–6475. IEEE, 2021.
- 380 [37] M. Sanderson. *Test collection based evaluation of information retrieval systems*. Now Pub-  
381 lishers Inc, 2010.